Use of quantum effects as potential qualifying metrics for "quantum grade silicon"

A. N. Ramanayaka,[1,2] Ke Tang,[1,2] J. A. Hagmann,[1] Hyun-Soo Kim,[1,2] D. S. Simons,[1] C. A. Richter,[1] and J. M. Pomeroy[1,a)]

[1)] *National Institute of Standards & Technology, Gaithersburg, Maryland 20899, USA*

[2)] *Joint Quantum Institute, University of Maryland, College Park, Maryland 20742, USA*

(Dated: 10 December 2019)

Across solid state quantum information, materials deficiencies limit performance through enhanced relaxation, charge defect motion or isotopic spin noise. While classical measurements of device performance provide cursory guidance, specific qualifying metrics and measurements applicable to quantum devices are needed. For quantum applications, new materials metrics, e.g., enrichment, are needed, while existing, classical metrics like mobility might be relaxed compared to conventional electronics. In this work, we examine locally grown silicon superior in enrichment, but inferior in chemical purity compared to commercial-silicon, as part of an effort to underpin the materials standards needed for quantum grade silicon and establish a standard approach for intercomparison of these materials. We use a custom, mass-selected ion beam deposition technique, which has produced isotopic enrichment levels up to 99.99998 % ^{28}Si, to isotopically enrich ^{28}Si, but with chemical purity $> 99.97\%$ due the MBE techniques used. From this epitaxial silicon, we fabricate top-gated Hall bar devices simultaneously on the ^{28}Si and on the adjacent natural abundance Si substrate for intercomparison. Using standard-methods, we measure maximum mobilities of $\approx (1740 \pm 2)$ cm^2/(V $\cdot$ s) at an electron density of $(2.7 \times 10^{12} \pm 3 \times 10^8)$ cm^{-2} and $\approx (6040 \pm 3)$ cm^2/(V $\cdot$ s) at an electron density of $(1.2 \times 10^{12} \pm 5 \times 10^8)$ cm^{-2} at $T = 1.9$ K for devices fabricated on ^{28}Si and $^{\mathrm{nat}}$Si, respectively. For magnetic fields $B > 2$ T, both devices demonstrate well developed Shubnikov-de Haas (SdH) oscillations in the longitudinal magnetoresistance. This provides transport characteristics of isotopically enriched ^{28}Si, and will serve as a benchmark for classical transport of ^{28}Si at its current state, and low temperature, epitaxially grown Si for quantum devices more generally.

Conventional electronics have been industrialized for decades; consequently, precise metrics based on macroscopic properties, such as chemical purity, charge carrier mobility, defect density, are established for qualifying a material, e.g., silicon, for conventional electronics. While silicon has been the work horse of conventional electronics, it also is becoming a promising host for spin based quantum information processing devices.[1,2] Specifically, spin qubits have already shown promising advancements with regard to long coherence times,[3,4] manipulation with high gate fidelity,[3,4] and scalability.[5,6]

Even though silicon has improved tremendously over the decades to meet demands of today's state-of-the-art transistors, this excellent material is still not sufficient to support quantum information. For example, in spin-based quantum information systems, the presence of the ^{29}Si isotope in natural abundance silicon reduces coherence times dues to the non-zero nuclear spin of $I = 1/2$. Nuclei with non-zero spin in the host lattice act as a source of decoherence for spin based qubits,[7] as they interact with the electron spin through hyperfine interactions.[8,9] However, by placing a spin qubit in an isotopically enriched 99.995 % ^{28}Si environment,[10] development of silicon based quantum devices have gained considerable momentum, with reports of exceptionally long quantum coherence times.[11,12]

The need for some level of enrichment provides an example of how "semiconductor grade" silicon quality may be necessary, but is not sufficient to meet the needs of quantum. Further, the metrics for conventional silicon may not always be relevant for quantum, e.g., the ease of carrier motion as quantified by mobility may not be directly relevant to quantum device performance where confinement and coherence in the *absence* of motion are critical. Additionally, as we establish properties and their numerical thresholds that are sufficient for quantum, relatively simple qualifying metrics that act as general proxies for properties more challenging to measure are invaluable. So, it may be that mobility in and of itself is not important, but it could be a good proxy for estimating spin-qubit relaxation or coherence.

As part of a larger program to identify and quantify "quantum grade" silicon, we are identifying 1) properties beyond those considered for semiconductor grade silicon critical to quantum; 2) the relevance and priority of properties currently considered critical for semiconductors; and 3) standard methods that may be used for new properties, or provide a general indicator for challenging properties, e.g., coherence time; as three main goals that are paramount for development of metrics for "quantum grade" silicon. This work is part of a broader effort to find ways besides making and measuring qubits to pro-

[a)] Correspondence to joshua.pomeroy@nist.gov

vide diagnostics that will indicate the likely performance of qubits early in a fabrication stream.

This paper presents devices, methods and results for a comparative study of magnetotransport properties between 1) high isotopic enrichment, low chemical purity and 2) high chemical purity, natural abundance (low isotopic enrichement) silicon. This characterization sets the stage for determining whether coherence properties in quantum dot devices correlate with the trends in these simpler measurements, since the benefit of enrichment on coherence may outpace the liability of some additional contaminants. In a detailed theoretical study, Witzel et al.,[13] illustrate that the coherence of a spin qubit can, in principle, be increased by an order of magnitude for every order of magnitude increase in the isotopic enrichment of ^{28}Si in the qubit's Si environment. A comprehensive experimental investigation of this prediction, however, is hindered due to the discreteness of the available isotopic enrichment levels. Among the four different enrichment levels have been reported[10,14–16] only 99.98% ^{28}Si[14] and 99.995% ^{28}Si[10] have been utilized for quantum electronic device fabrication.[11,17,18] Moreover, contemporary methods for producing isotopically enriched ^{28}Si material are based on chemical vapor deposition (CVD) techniques and are not compatible with qubit architectures requiring low temperature processing, e.g. STM fabricated single dopant atom qubits.[19] In contrast, the method used for producing ^{28}Si reported here is compatible with all the contemporary qubit architectures, and represents molecular beam epitaxy (MBE) grown Si more generally. While the coherence of a spin qubit is predicted to improve at higher isotopic enrichment levels,[13] how other material properties will limit the expected enhancement of qubit coherence is unclear. To the best of our knowledge, no study yet has attempted to correlate macroscopic electrical characteristics to the performance of quantum devices. Yet such a study will be an essential component for defining metrics for "quantum grade" silicon within the three main goals identified earlier.

Starting from natural abundance SiH_4 gas, we have developed a method to grow isotopically purified silicon reaching isotopic enrichments up to 99.99998 % ^{28}Si.[20,21] This method provides the unique advantage of targeting a desired enrichment level anywhere from natural abundance to the highest possible enrichment.[22] As a first step towards correlating macroscopic electrical characteristics with the performance of quantum devices, we report here on characterization of gated Hall bar devices fabricated on isotopically enriched ^{28}Si, and control devices on the same natural abundance Si (^{nat}Si) substrate but outside the isotopically enriched ^{28}Si spot using macroscopic manifestations of quantum effects such as Shubnikov-de Haas (SdH) effect and weak-localization effect. We compare the devices fabricated on ^{nat}Si (float-zone grown) and ^{28}Si (MBE grown) during the same fabrication process, eliminating possible differences due to imperfect fabrication conditions. We present results of ^{28}Si devices to serve as a benchmark for MBE grown isotopically enriched ^{28}Si, and a basis for comparing macroscopic electrical characteristics within silicon quantum electronics.

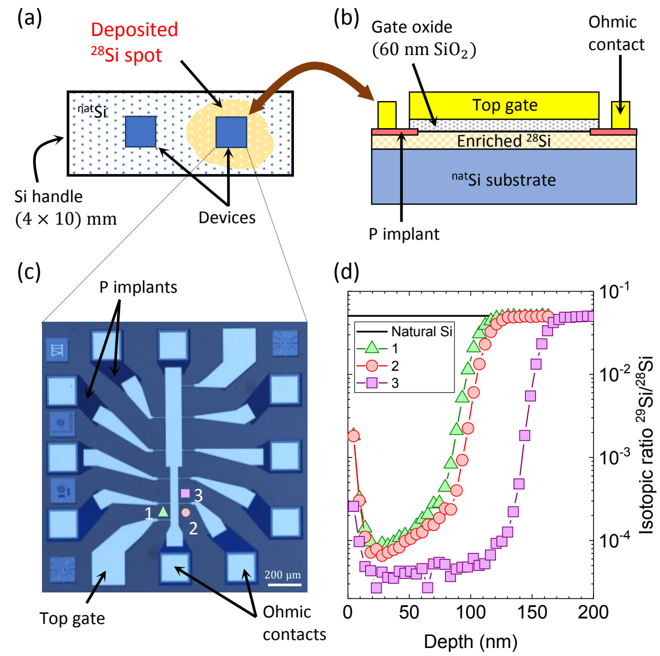

FIG. 1. (a) A schematic illustrating the device layout of a given sample. Reduced coverage of the ^{28}Si spot allows to fabricate devices on ^{28}Si and ^{nat}Si simultaneously. (b) Schematic representation of the gated Hall bar device fabricated on ^{28}Si is shown. (c) An optical micrograph of a gated multi-terminal Hall bar device fabricated on ^{28}Si is shown.(d) The isotopic ratios of ^{29}Si/^{28}Si at positions 1 (△), 2 (◯), and 3 (□) in (c) are shown. The shift in the rising edge at different positions corresponds to the thickness variation in the deposited ^{28}Si film. Measured ^{29}Si isotopic ratios at locations 1, 2, and 3 are $(149 \pm 18) \times 10^{-6}$ mol/mol, $(128 \pm 14) \times 10^{-6}$ mol/mol, and $(45 \pm 2) \times 10^{-6}$ mol/mol, respectively.

Starting with 99.999 % pure, commercially available, natural isotopic abundance SiH_4 gas, isotopically enriched ^{28}Si is grown using a hyperthermal energy ion beam deposition system[20]. Gated Hall bar devices are fabricated on isotopically enriched ^{28}Si epilayers in order to electrically characterize the material. Typically, the isotopically purified ^{28}Si spot is ≈ 2 mm^2 to 3 mm^2 in area and covers only a small fraction of the starting float-zone grown, natural abundance, intrinsic Si substrate (4 mm × 10 mm), see Fig. 1(a). Due to the reduced coverage of the ^{28}Si spot, devices on isotopically enriched and natural abundance Si can be fabricated on the same Si chip [see Fig. 1(a)] at the same time. This eliminates the effect of imperfections in the fabrication process (e.g., oxide growth) when comparing the electrical properties of the devices. A schematic cross section of a device fabricated on ^{28}Si spot is shown in Fig. 1(b). The structure of the devices fabricated on ^{nat}Si, i.e. outside the ^{28}Si spot, is identical except without the ^{28}Si

TABLE I. Macroscopic materials and electrical properties of natural abundance, $^{\mathrm{nat}}$Si, and isotopically enriched, ^{28}Si, silicon.

Property		Material $^{\mathrm{nat}}$Si	^{28}Si
Avg. ^{28}Si concentration		92.23 %	99.983 %
Impurities (cm^{-3})	C		2×10^{19}
	N	$\leq 10^{16}$	3×10^{17}
	O		3×10^{18}
Max. mobility μ (cm^2/(V $\cdot$ s))		(6040 ± 3)	(1740 ± 2)
Percolation density n_p (10^{11} cm^{-2})		(2.3 ± 2)	(4.2 ± 2)

layer. An optical micrograph of the gated multi-terminal Hall bar device is shown in Fig. 1(c).

The isotopic enrichment of the ^{28}Si epilayers is measured by using Secondary Ion Mass Spectrometry (SIMS). In Fig. 1(d), the SIMS-derived isotopic ratio of ^{29}Si/^{28}Si is shown as a function of depth at several locations near the fabricated Hall bar device. For the device reported here, the level of isotopic enrichment measured at locations 1, 2, and 3 corresponds to ≈ 99.976 %, ≈ 99.980 %, and ≈ 99.993 % ^{28}Si, respectively. Figure 1(d) also reveals the thickness non-uniformity of the deposited ^{28}Si epilayer, i.e., the thickness of the ^{28}Si epilayer at location 3 is greater than that of locations 1 and 2. Moreover, separate SIMS measurements on these isotopically enriched ^{28}Si epilayers reveals that the films contain adventitious chemical impurities, namely C, N, O, with approximate atomic concentrations of 2×10^{19} cm^{-3}, 3×10^{17} cm^{-3}, and 3×10^{18} cm^{-3}. However, the atomic concentrations of these chemical impurities on the handle wafer were below the SIMS detection limit ($\leq 10^{16}$ cm^{-3}). We believe that these chemical impurities are being introduced by the ion beam as result of non-UHV compatible ionization source that is used to create the ion beams during the ^{28}Si deposition, and since been upgraded.

The magnetoresistance (R_{xx}) and the Hall resistance (R_{xy}) at 1.9 K for isotopically enriched ^{28}Si and natural abundance Si are shown in Fig. 2(a) and Fig. 2(b), respectively. Using low field magnetotransport data, we find maximum mobilities at $T = 1.9$ K for ^{28}Si and $^{\mathrm{nat}}$Si are, respectively, $\mu_{^{28}\mathrm{Si}} = (1740\pm2)$ cm^2/(V $\cdot$ s) at an electron density n of $(2.7\times10^{12}\pm3\times10^{8})$ cm^{-2} and $\mu_{^{\mathrm{nat}}\mathrm{Si}} = (6040\pm3)$ cm^2/(V $\cdot$ s) at an electron density of $(1.2\times10^{12}\pm5\times10^{8})$ cm^{-2}. Charge carrier mobilities for these devices are within the typical range of mobilities for Si-MOS (Metal Oxide Semiconductor) devices fabricated using non-MBE (e.g. CVD) growth techniques,[23,24] the maximum mobility for a Si-MOS device to date being $> 4\times10^4$ cm^2/(V $\cdot$ s)[25]. In contrast, mobilities reported for Si-MOS devices fabricated on MBE grown Si ranges from 900 cm^2/(V $\cdot$ s) to 1250 cm^2/(V $\cdot$ s)[26,27].

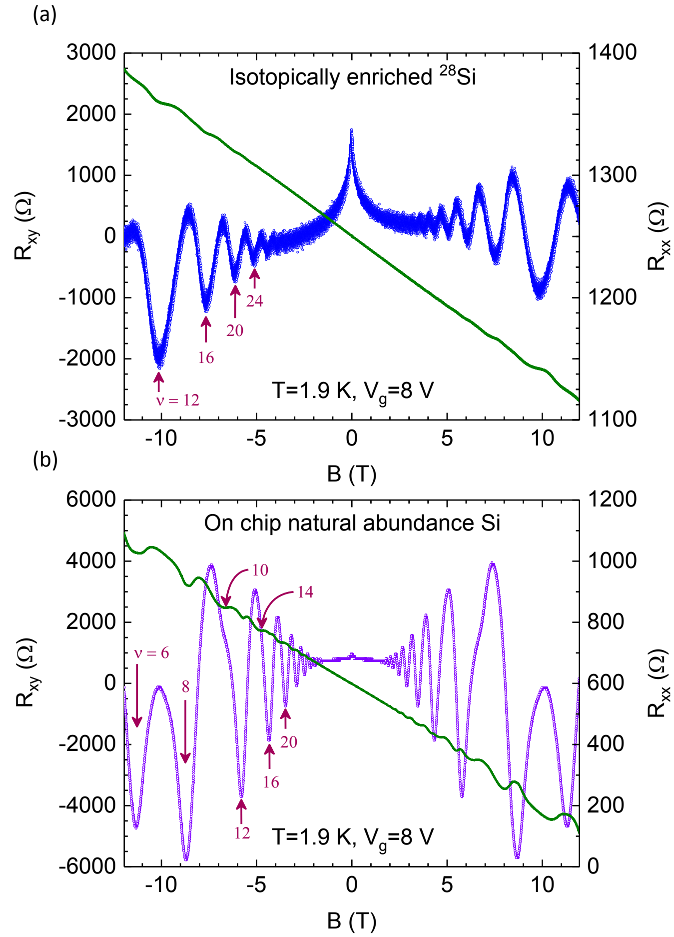

FIG. 2. The magnetoresistance R_{xx} (right-axis) and the Hall resistance R_{xy} (left-axis) measured for the devices fabricated on (a) isotopically enriched ^{28}Si epi-layer, and (b) natural Si substrate are shown. For both devices, the corresponding filling factors (ν) are shown at the minima of Shubnikov-de Hass oscillations. In contrast to the device on isotopically enriched ^{28}Si epi-layer, the device on $^{\mathrm{nat}}$Si demonstrates spin-splitting for $B > 3$ T. Both devices are fabricated on the same Si chip, see main text for more information. The relative uncertainty associated with R_{xx} and R_{xy} is typically less than 0.1 % and is mostly due to the uncertainty of the measured current.

In order to estimate the percolation electron density n_p, we extrapolate the electron density as a function of gate voltage (as determined from Hall measurements) back to the threshold voltage (as determined from the channel current I_{sd} vs. V_g), i.e., $n_p = n_e(V_{th})$. Using this method, we find percolation densities of $(2.3\pm2)\times10^{11}$ cm^{-2} for $^{\mathrm{nat}}$Si and $(4.2\pm2)\times10^{11}$ cm^{-2} for ^{28}Si. While the relative uncertainties are large due to the extrapolation, we think the $\approx 2\times$ larger value for ^{28}Si is significant. A summary of these macroscopic materials and electrical properties for the on-chip $^{\mathrm{nat}}$Si and ^{28}Si is provided in table I.

Both devices show well developed SdH oscillations in R_{xx} with accompanying plateaus in R_{xy}. The slight asymmetry in R_{xx} in Fig. 2(a) could be due to several reasons, e.g., magnetic impurities or inhomogeneity of the magnetic field.[28,29] The SIMS of a similar ^{28}Si epilayer found no measurable magnetic impurities. The Hall resistance shows non-idealities particularly in the $^{\mathrm{nat}}$Si device [Fig. 2(b)] where R_{xy} is non-monotonic. These non-idealities could be due to scattering between discrete degenerate states at the tails due to level broadening.[30,31] However, a detailed discussion of the asymmetry of R_{xx} and the flatness of the Hall plateaus is outside the scope of this article. We also see a lifting of the four-fold degeneracy at $B > 5$ T for $^{\mathrm{nat}}$Si, which is likely due to the spin degree of freedom, but, at this time we are unable to determine whether this is due to spin or valley degree of freedom, due to limitations in the experimental setup.

Near zero magnetic field, both devices demonstrate a peak in the sample resistance, see Fig. 2. This increase in resistance near zero magnetic field is known as weak localization (WL). Weak localization is a quantum mechanical phenomenon that can be observed in two-dimensional (2D) electron systems at low temperatures where the phase coherence length (l_ϕ) is greater than the mean free path (l)[32,33]. Relative to the zero field resistance, the weak-localization is larger for the device fabricated on isotopically enriched ^{28}Si.

To further investigate the WL behavior of these devices, we plot the change in conductivity $\Delta\sigma_{xx}$ as a function of magnetic field B applied perpendicular to the 2D electron system [see Fig. 3]. The change in conductivity due to WL $\Delta\sigma_{xx} = \sigma_{xx}(B) - \sigma_{xx}(B = 0)$, where $\sigma_{xx} = \rho_{xx}/(\rho_{xx}^2 + \rho_{xy}^2)$. For non-zero B, the change in conductivity due to WL in a 2D electron system can be modeled by the Hikami-Larkin-Nagaoka (HLN) equation,[34]

$$\begin{aligned}\Delta\sigma_{xx}(B) =& \alpha\Big(\frac{e^2}{2\pi^2\hbar}\Big)\Big[\Psi\Big(\frac{1}{2}+\frac{\hbar}{4el_\phi^2 B}\Big) \\ & -\Psi\Big(\frac{1}{2}+\frac{\hbar}{2el^2 B}\Big) - \ln\Big(\frac{l}{2l_\phi}\Big)\Big], \qquad (1)\end{aligned}$$

where Ψ is the digamma function, l is the mean free path, l_Φ is the phase coherence length, and α is a constant close to unity. In Fig. 3, the solid lines are the fits to experimental data (symbols) using the HLN equation. For these fits, we use the calculated values of l using the relation $l = \sqrt{2D\tau}$. Here D is the diffusion coefficient defined as $D = v_F^2\tau/2$, where the Fermi velocity $v_F = \hbar k_F/m^*$, and τ is the elastic scattering time, also known as transport lifetime, defined as $\tau = \mu m^*/e$. The effective mass m^* is defined as $m^*/m_0 = 0.19$, where m_0 is the rest mass of an electron.[35,36] The Fermi wavelength k_F can be calculated for a 2D electron system in Si as $k_F = (4\pi n_{2D}/g_s g_v)^{1/2}$, where n_{2D}, g_s, g_v are the charge carrier density, spin degeneracy and valley degeneracy, respectively. We leave α and l_ϕ as free fitting parameters, constraining the value of α to be close to unity. From the fit-extracted values of l_ϕ, we calculate $1/\tau_\phi$, where inelastic scattering time $\tau_\phi = l_\phi^2/D$. The fit derived values of $1/\tau_\phi$ as a function of T are plotted in Fig.3 inset for devices fabricated on isotopically enriched ^{28}Si and natural abundance Si, respectively. The solid lines in Fig. 3 inset are the least-squares-fit to the data using the equation

$$\frac{1}{\tau_\phi} = a + bT + cT^2. \qquad (2)$$

The linear in T term captures the scattering from impurities, and the quadratic in T term is related to the electron-electron scattering.[37] Table II shows the parameters extracted from the least-squares-fit to the data, the fit uncertainties for both devices, and the adjusted R-

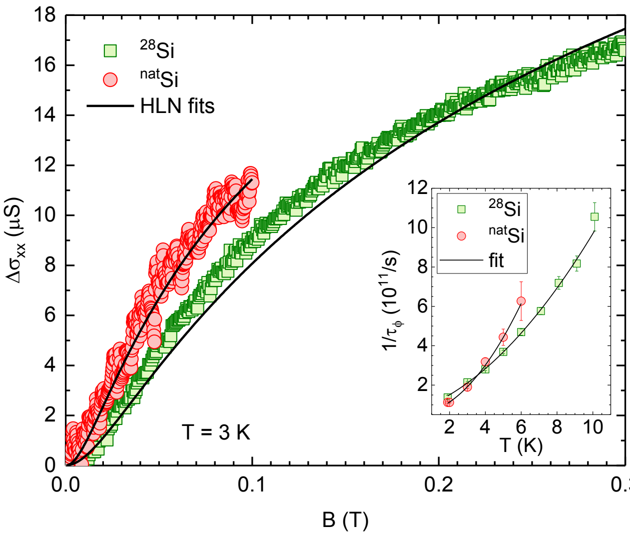

FIG. 3. The change in conductivity ($\Delta\sigma_{xx}$) vs external magnetic field (B) for devices fabricated on ^{28}Si (□) and $^{\mathrm{nat}}$Si (◯) measured at 3 K. Solid lines are the least-square-fits to HLN equation (Eq. 1). Estimated uncertainty for $\Delta\sigma_{xx}$ is < 0.3 %. Inset: The inelastic scattering rates ($1/\tau_\phi$) for ^{28}Si and $^{\mathrm{nat}}$Si vs the measurement temperature are shown. Here the solid lines are the least-squares-fit to a quadratic equation, see main text details. Error bars in the inset represent the fit uncertainty associated with the values extracted for $1/\tau_\phi$ at each temperature.

TABLE II. Parameters extracted from the least-squares-fits of Eq. 2 to the data in Fig. 3 inset.

Device	a (10^{10} s^{-1})	b (10^{10} K^{-1}s^{-1})	c (10^{10} K^{-2}s^{-1})	Adjusted R-square
^{28}Si	6.6 ± 2	3.1 ± 0.7	0.60 ± 0.08	0.997
$^{\mathrm{nat}}$Si	5.1 ± 0.4	-	1.5 ± 0.1	0.989

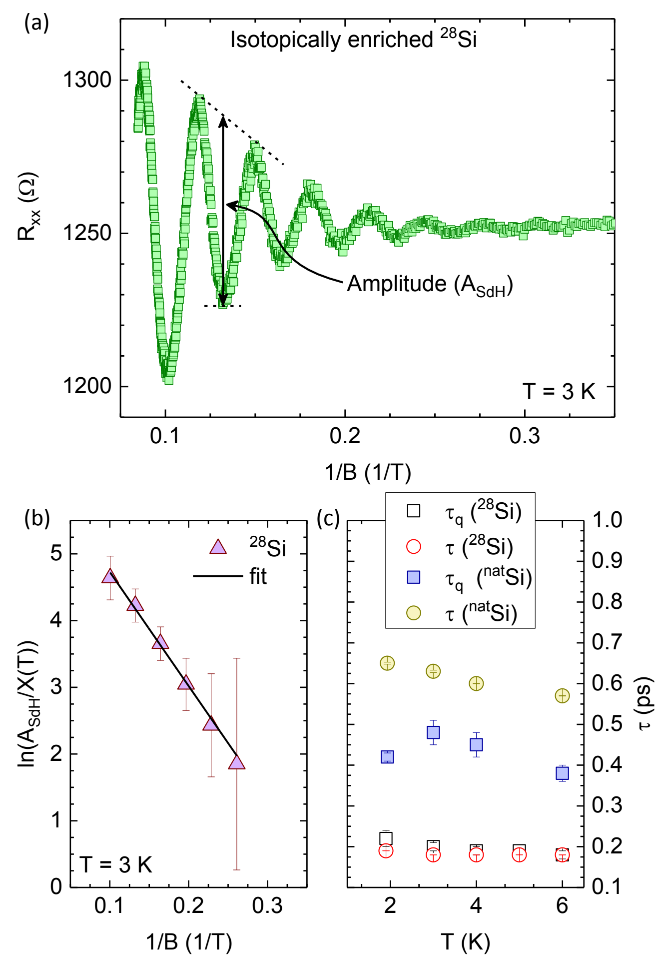

FIG. 4. (a) The background subtracted (see text) R_{xx}, i.e., ΔR_{xx}, vs the inverse of the external magnetic field ($1/B$) for the ^{28}Si device is shown. (b) A "Dingle plot" of $\ln(A_{SdH}/X(T))$ versus $1/B$. Error bars represent the uncertainty associated with extracting A_{SdH} from ΔR_{xx} vs. $1/B$ plot. (c) The single particle lifetimes, τ_q, extracted from the Dingle plots and transport lifetimes, τ, at different temperatures for devices on ^{28}Si and $^{\mathrm{nat}}$Si. Error bars represent the uncertainty associated with calculating the values of τ_q (τ) using the Dingle plots (charge carrier mobilities) at each temperature.

square. For the natural abundance Si, the best fit is achieved when the linear term is set to zero, i.e., $b = 0$. Consequently, for natural abundance Si the dominant scattering mechanism appears to be the electron-electron (long-range) scattering. In contrast, for isotopically enriched ^{28}Si, the best fit is achieved with a significant linear in T term. This large linear term implies that impurity (short-range) scattering is a significant contribution in ^{28}Si. The temperature independent parameter a is similar (within the uncertainties) for both the devices indicating the processes (e.g., interface roughness) contributing to a are likely the same.

Line shape analysis of the SdH oscillations as a function of temperature is also used to investigate the underlying scattering mechanisms in 2D electron systems. The amplitude of the SdH oscillations can be written as $A_{SdH} = X(T)R_0\exp(-\pi/\omega_c\tau_q)$[38,39], where R_0 is the zero field resistance, $X(T) = (2\pi^2 k_B T/\hbar\omega_c)/\sinh(2\pi^2 k_B T/\hbar\omega_c)$ is the temperature damping factor, and $\omega_c = eB/m^*$ is the cyclotron frequency. Here, k_B is Boltzmann's constant, and τ_q is the single particle (quantum) lifetime.[38–40] To extract the amplitude of SdH oscillations, we first subtract a slow varying background from R_{xx}[41] to isolate the oscillatory part of R_{xx}. The R_{xx} after background subtraction (ΔR_{xx}) is plotted against $1/B$ in Fig. 4(a). Then we extract the amplitude A_{SdH} as schematically defined in Fig. 4(a) at each minima of ΔR_{xx} and calculate $\ln(A_{SdH}/X(T))$. Figure 4(b) is a plot of $\ln(A_{SdH}/X(T))$ versus $1/B$, also known as the "Dingle plot"[38,39] for the device fabricated on ^{28}Si measured at $T = 3$ K. The approximately linear dependence of $\ln(A_{SdH}/X(T))$ on $1/B$ [see Fig. 4 (b)] indicates a magnetic field independent quantum lifetime, τ_q. In Fig. 4 (c), we plot the quantum lifetimes, τ_q, for devices fabricated on ^{28}Si and $^{\mathrm{nat}}$Si extracted from a linear least-squares-fit to Dingle plots at each temperature. The calculated values of the transport lifetimes, where $\tau = \mu m^*/e$, using the magnetotransport measurement at low magnetic fields for both devices, are also plotted in Fig. 4 (c).

For the device fabricated on ^{28}Si, the ratio of $\tau/\tau_q \approx 1$, and for the device on $^{\mathrm{nat}}$Si the ratio of $\tau/\tau_q \approx 1.4$. The transport lifetime τ is primarily affected by the large angle scattering events that cause large momentum change, whereas τ_q is affected by all of the scattering events[42]. When the background impurities dominate the scattering the ratio τ/τ_q is less than or equal to 10, whereas it is ≈ 1 when the scattering is dominated by short-range isotropic scattering[42], e.g. surface roughness scattering[43]. The thickness of the gate oxide for the devices reported here is ≈ 60 nm. We therefore neglect the scattering due to remote interface roughness (i.e., the interface between the gate oxide and the gate metal) as a dominant scattering mechanism for these devices.[44] Therefore, the ratio τ/τ_q implies that the charge carrier mobility is limited by the background impurity scattering. Furthermore, the charge carrier mobility of the device on isotopically enriched ^{28}Si may also be limited by the interface roughness scattering.

The analysis of the weak-localization, SdH oscillations, and low-field magnetotransport data indicate that the shortest scattering length scale to be the elastic (transport) scattering length l calculated, ≈ 33 nm and ≈ 71 nm for ^{28}Si and $^{\mathrm{nat}}$Si, respectively. Capacitance voltage (CV) measurements of MOS capacitors fabricated on natural abundance silicon (data not shown) with gate oxides grown using similar conditions to the devices reported here reveals a fixed charge density of approximately 3×10^{10} cm^{-2} corresponding to a nearest neighbor distance of ≈ 58 nm. This nearest neighbor distance is in close agreement with the transport scattering length

l. Considering SIMS measured chemical impurity concentrations of C, N, and O and assuming these impurities acting as isolated scatters, for ^{28}Si where $l \approx 33$ nm, we estimate the fraction of C, N, and O impurities contributing to scattering to be ≈ 0.2 %, ≈ 9.3 % and ≈ 1.0 %, respectively.

In conclusion, we have reported on the first low temperature electrical measurements of MBE grown isotopically enriched ^{28}Si. For this report we fabricated and characterized the low temperature magnetotransport of gated Hall bar devices fabricated on highly enriched ^{28}Si. In comparison to control devices fabricated on float-zone grown, intrinsic, natural abundance Si on the same substrate, the charge carrier mobility on isotopically enriched ^{28}Si is approximately a factor of 3 lower. Nevertheless, the magnetotransport measurements of devices fabricated on isotopically enriched ^{28} Si demonstrate strong manifestations of quantum effects. Based on the analysis of temperature dependence of the weak localization and SdH oscillations, we believe that the dominant scattering mechanism is short-range scattering (impurity scattering). We believe adventitious chemical impurities detected in the ^{28}Si epilayers act as the impurity scatters in the devices fabricated on ^{28}Si. However, higher levels of adventitious chemical impurities detected in the ^{28}Si epilayers are too high to be considered as isolated scattering centers, since the nearest neighbor distance is considerably shorter than the scattering lengths extracted from the transport data. Further, for these impurity levels, the dipolar interactions between randomly distributed electron spins associated with impurities and the central spin of a potential qubit is considered to be the dominant decoherence mechanism at high enrichments.[13] For the worst case analysis, if all of the N and O chemical impurities are considered as randomly distributed single electron spins, the influence of these dipolar interactions on the central spin could result in qubit coherence times poorer than high purity natural abundance Si. However, we are confident that the recent and planned improvements, as well as techniques for depleting impurities near the surfaces, will allow us to move forward and study the tension between chemical impurites and enrichement on quantum coherence.

Next we plan to fabricate quantum dot devices on control (natural abundance) and isotopically enriched ^{28}Si to more rigorously assess the impact of purity and enrichment, e.g. charge offset drift, as the chemical purity of these MBE grown ^{28}Si films is improved. Therefore, macroscopic transport and material characteristics of the devices reported here will serve as a benchmark for finding the correlations between macroscopic properties and the performance of future nanoscale devices, e.g. quantum dots, and lead to identifying qualifying metrics for "quantum grade" silicon.

ACKNOWLEDGMENTS

The authors acknowledge stimulating discussions with Michael Stewart, Neil Zimmerman, Roy Murray, Ryan Stein, Binhui Hu, and Peihao Huang.

[1] D. Loss and D. P. DiVincenzo, "Quantum computation with quantum dots," Phys. Rev. A **57**, 120–126 (1998).

[2] J. J. L. Morton, D. R. McCamey, M. A. Eriksson, and S. A. Lyon, "Embracing the quantum limit in silicon computing," Nature **479**, 345–353 (2011).

[3] M. Veldhorst, J. C. C. Hwang, C. H. Yang, A. W. Leenstra, B. de Ronde, J. P. Dehollain, J. T. Muhonen, F. E. Hudson, K. M. Itoh, A. Morello, and A. S. Dzurak, "An addressable quantum dot qubit with fault-tolerant control-fidelity," Nature Nanotechnology **9**, 981 (2014).

[4] J. Yoneda, K. Takeda, T. Otsuka, T. Nakajima, M. R. Delbecq, G. Allison, T. Honda, T. Kodera, S. Oda, Y. Hoshi, N. Usami, K. M. Itoh, and S. Tarucha, "A quantum-dot spin qubit with coherence limited by charge noise and fidelity higher than 99.9%," Nature Nanotechnology **13**, 102–106 (2018).

[5] D. M. Zajac, T. M. Hazard, X. Mi, E. Nielsen, and J. R. Petta, "Scalable gate architecture for a one-dimensional array of semiconductor spin qubits," Phys. Rev. Applied **6**, 054013 (2016).

[6] D. M. Zajac, A. J. Sigillito, M. Russ, F. Borjans, J. M. Taylor, G. Burkard, and J. R. Petta, "Resonantly driven CNOT gate for electron spins," Science **359**, 439–442 (2018).

[7] J. P. Gordon and K. D. Bowers, "Microwave spin echoes from donor electrons in silicon," Phys. Rev. Lett. **1**, 368–370 (1958).

[8] J. R. Petta, A. C. Johnson, J. M. Taylor, E. A. Laird, A. Yacoby, M. D. Lukin, C. M. Marcus, M. P. Hanson, and A. C. Gossard, "Coherent manipulation of coupled electron spins in semiconductor quantum dots," Science **309**, 2180–2184 (2005).

[9] D. J. Reilly, J. M. Taylor, J. R. Petta, C. M. Marcus, M. P. Hanson, and A. C. Gossard, "Suppressing spin qubit dephasing by nuclear state preparation," Science **321**, 817–821 (2008).

[10] P. Becker, H.-J. Pohl, H. Riemann, and N. Abrosimov, "Enrichment of silicon for a better kilogram," physica status solidi (a) **207**, 49–66 (2009).

[11] K. Saeedi, S. Simmons, J. Z. Salvail, P. Dluhy, H. Riemann, N. V. Abrosimov, P. Becker, H.-J. Pohl, J. J. L. Morton, and M. L. W. Thewalt, "Room-temperature quantum bit storage exceeding 39 minutes using ionized donors in silicon-28," Science **342**, 830–833 (2013).

[12] M. Steger, K. Saeedi, M. L. W. Thewalt, J. J. L. Morton, H. Riemann, N. V. Abrosimov, P. Becker, and H.-J. Pohl, "Quantum information storage for over 180 s using donor spins in a ^{28}Si "semiconductor vacuum"," Science **336**, 1280–1283 (2012).

[13] W. M. Witzel, M. S. Carroll, A. Morello, L. Cywiński, and S. Das Sarma, "Electron spin decoherence in isotope-enriched silicon," Phys. Rev. Lett. **105**, 187602 (2010).

[14] K. M. Itoh, J. Kato, M. Uemura, A. K. Kaliteevskii, O. N. Godisov, G. G. Devyatych, A. D. Bulanov, A. V. Gusev, I. D. Kovalev, P. G. Sennikov, H.-J. Pohl, N. V. Abrosimov, and H. Riemann, "High purity isotopically enriched ^{29}Si and ^{30}Si single crystals: Isotope separation, purification, and growth," Japanese Journal of Applied Physics **42**, 6248 (2003).

[15] L. Petit, J. M. Boter, H. G. J. Eenink, G. Droulers, M. L. V. Tagliaferri, R. Li, D. P. Franke, K. J. Singh, J. S. Clarke, R. N. Schouten, V. V. Dobrovitski, L. M. K. Vandersypen, and M. Veldhorst, "Spin lifetime and charge noise in hot silicon quantum dot qubits," Phys. Rev. Lett. **121**, 076801 (2018).

[16] V. Mazzocchi, P. G. Sennikov, A. D. Bulanov, M. F. Churbanov, B. Bertrand, L. Hutin, J. P. Barnes, M. N. Drozdov, J. M. Hartmann, and M. Sanquer, "99.992 % ^{28}Si CVD grown epilayer on 300 mm substrates for large scale integration of silicon spin qubits," Journal of Crystal Growth **509**, 1–7 (2019).

[17] J. T. Muhonen, J. P. Dehollain, A. Laucht, F. E. Hudson, R. Kalra, T. Sekiguchi, K. M. Itoh, D. N. Jamieson, J. C. Mc-

Callum, A. S. Dzurak, and A. Morello, "Storing quantum information for 30 seconds in a nanoelectronic device," Nature Nanotechnology **9**, 986 (2014).

[18]L. A. Tracy, D. R. Luhman, S. M. Carr, N. C. Bishop, G. A. Ten Eyck, T. Pluym, J. R. Wendt, M. P. Lilly, and M. S. Carroll, "Single shot spin readout using a cryogenic high-electron-mobility transistor amplifier at sub-Kelvin temperatures," Applied Physics Letters **108**, 063101 (2016).

[19]M. Koch, J. G. Keizer, P. Pakkiam, D. Keith, M. G. House, E. Peretz, and M. Y. Simmons, "Spin read-out in atomic qubits in an all-epitaxial three-dimensional transistor," Nature Nanotechnology **14**, 137–140 (2019).

[20]K. J. Dwyer, J. M. Pomeroy, D. S. Simons, K. L. Steffens, and J. W. Lau, "Enriching ^{28}Si beyond 99.9998 % for semiconductor quantum computing," Journal of Physics D: Applied Physics **47**, 345105 (2014).

[21](), Highest isotopic enrichment measured to date is 99.99998 % ^{28}Si, and are planned for future publication. Data can be made available upon a reasonable request.

[22](), Targeted enrichment results will be published soon.

[23]F. A. Zwanenburg, A. S. Dzurak, A. Morello, M. Y. Simmons, L. C. L. Hollenberg, G. Klimeck, S. Rogge, S. N. Coppersmith, and M. A. Eriksson, "Silicon quantum electronics," Rev. Mod. Phys. **85**, 961–1019 (2013).

[24]R. Pillarisetty, N. Thomas, H. C. George, K. Singh, J. Roberts, L. Lampert, P. Amin, T. F. Watson, G. Zheng, J. Torres, M. Metz, R. Kotlyar, P. Keys, J. M. Boter, J. P. Dehollain, G. Droulers, G. Eenink, R. Li, L. Massa, D. Sabbagh, N. Samkharadze, C. Volk, B. P. Wuetz, A. . Zwerver, M. Veldhorst, G. Scappucci, L. M. K. Vandersypen, and J. S. Clarke, "Qubit device integration using advanced semiconductor manufacturing process technology," in *2018 IEEE International Electron Devices Meeting (IEDM)* (2018) pp. 6.3.1–6.3.4.

[25]S. V. Kravchenko and M. P. Sarachik, "Metal-insulator transition in two-dimensional electron systems," Reports on Progress in Physics **67**, 1 (2004).

[26]Y. Ota, "Silicon molecular beam epitaxy," Thin Solid Films **106**, 1 – 136 (1983).

[27]R. G. Swartz, G. M. Chin, A. M. Voshchenkov, P. Ko, B. A. Wooley, S. N. Finegan, and R. H. Bosworth, "Digital NMOS test circuits fabricated in silicon MBE," IEEE Electron Device Letters **5**, 29–31 (1984).

[28]M. L. Leadbeater, C. L. Foden, J. H. Burroughes, M. Pepper, T. M. Burke, L. L. Wang, M. P. Grimshaw, and D. A. Ritchie, "Magnetotransport in a nonplanar two-dimensional electron gas," Phys. Rev. B **52**, R8629–R8632 (1995).

[29]A. B. Vorob'ev, K.-J. Friedland, H. Kostial, R. Hey, U. Jahn, E. Wiebicke, J. S. Yukecheva, and V. Y. Prinz, "Giant asymmetry of the longitudinal magnetoresistance in high-mobility two-dimensional electron gas on a cylindrical surface," Phys. Rev. B **75**, 205309 (2007).

[30]S. Komiyama and H. Hirai, "Theory of contacts in a two-dimensional electron gas at high magnetic fields," Phys. Rev. B **40**, 7767–7775 (1989).

[31]C. T. V. Degrift, K. Yoshihiro, E. C. Palm, J. Wakabayashi, and S. Kawaji, "Re-examination of quantum Hall plateaus," IEEE Transactions on Instrumentation and Measurement **42**, 562–567 (1993).

[32]P. A. Lee and T. V. Ramakrishnan, "Disordered electronic systems," Rev. Mod. Phys. **57**, 287–337 (1985).

[33]J. A. Hagmann, X. Wang, P. Namboodiri, J. Wyrick, R. Murray, M. D. Stewart, R. M. Silver, and C. A. Richter, "High resolution thickness measurements of ultrathin Si:P monolayers using weak localization," Applied Physics Letters **112**, 043102 (2018).

[34]S. Hikami, A. I. Larkin, and Y. Nagaoka, "Spin-orbit interaction and magnetoresistance in the two dimensional random system," Progress of Theoretical Physics **63**, 707–710 (1980).

[35]T. Ando, A. B. Fowler, and F. Stern, "Electronic properties of two-dimensional systems," Rev. Mod. Phys. **54**, 437–672 (1982).

[36]S. M. Sze and K. K. Ng, *Physics of Semiconductor Devices.*, Vol. 3rd ed (Wiley-Interscience, 2007).

[37]R. A. Davies and M. Pepper, "Electron-electron scattering in silicon inversion layers," Journal of Physics C: Solid State Physics **16**, L353 (1983).

[38]M. Padmanabhan, T. Gokmen, N. C. Bishop, and M. Shayegan, "Effective mass suppression in dilute, spin-polarized two-dimensional electron systems," Phys. Rev. Lett. **101**, 026402 (2008).

[39]X. Mi, T. M. Hazard, C. Payette, K. Wang, D. M. Zajac, J. V. Cady, and J. R. Petta, "Magnetotransport studies of mobility limiting mechanisms in undoped Si/SiGe heterostructures," Phys. Rev. B **92**, 035304 (2015).

[40]R. G. Mani, W. B. Johnson, V. Umansky, V. Narayanamurti, and K. Ploog, "Phase study of oscillatory resistances in microwave-irradiated- and dark-GaAs/AlGaAs devices: Indications of an unfamiliar class of the integral quantum hall effect," Phys. Rev. B **79**, 205320 (2009).

[41]P. T. Coleridge, "Inter-subband scattering in a 2D electron gas," Semiconductor Science and Technology **5**, 961–966 (1990).

[42]S. J. MacLeod, K. Chan, T. P. Martin, A. R. Hamilton, A. See, A. P. Micolich, M. Aagesen, and P. E. Lindelof, "Role of background impurities in the single-particle relaxation lifetime of a two-dimensional electron gas," Phys. Rev. B **80**, 035310 (2009).

[43]A. Gold, "Scattering time and single-particle relaxation time in a disordered two-dimensional electron gas," Phys. Rev. B **38**, 10798–10811 (1988).

[44]J. Li and T. Ma, "Scattering of silicon inversion layer electrons by metal/oxide interface roughness," Journal of Applied Physics **62**, 4212–4215 (1987).

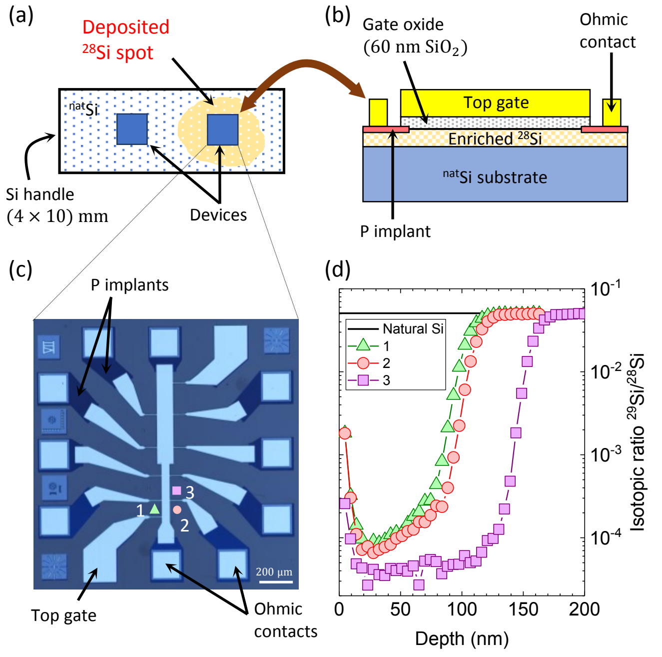

(a)
Deposited
^{28}Si spot
^{nat}Si
Si handle
(4 × 10) mm
Devices
(b)
Gate oxide
(60 nm SiO_2)
Ohmic
contact
Top gate
Enriched ^{28}Si
^{nat}Si substrate
P implant
(c)
P implants
1
2
3
200 μm
Top gate
Ohmic
contacts
(d)
Natural Si
1
2
3
Isotopic ratio ^{29}Si/^{28}Si
Depth (nm)
0
50
100
150
200
10^{-1}
10^{-2}
10^{-3}
10^{-4}

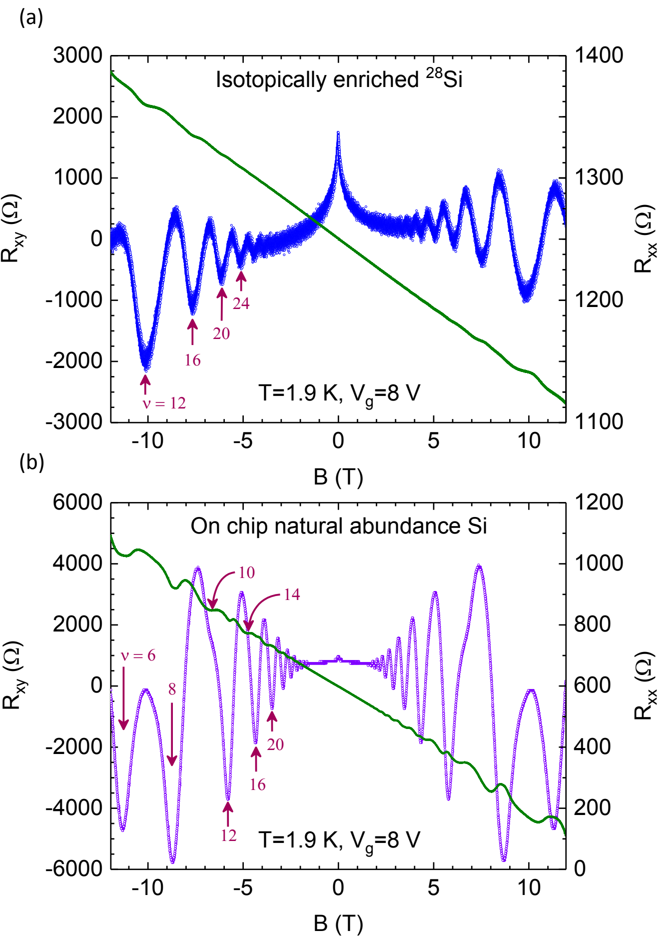
(a)
Isotopically enriched ^{28}Si
T=1.9 K, V_g=8 V
ν = 12
16
20
24
R_{xy} (Ω)
R_{xx} (Ω)
B (T)
(b)
On chip natural abundance Si
T=1.9 K, V_g=8 V
ν = 6
8
10
12
14
16
20
R_{xy} (Ω)
R_{xx} (Ω)
B (T)

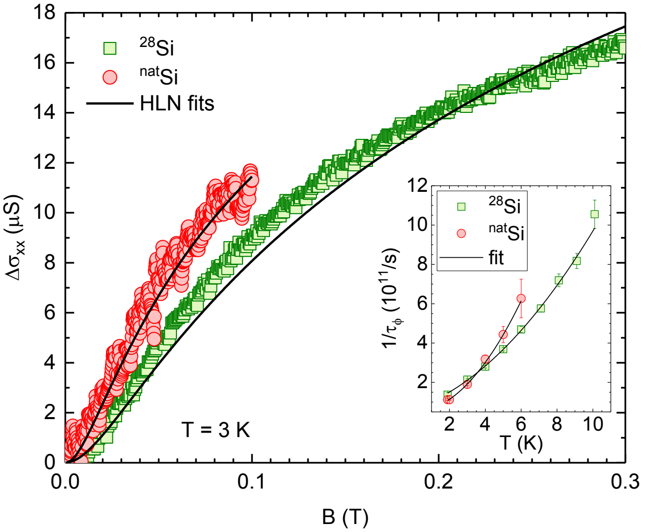

28Si
natSi
HLN fits
T = 3 K
Δσxx (μS)
B (T)
0.0
0.1
0.2
0.3
0
2
4
6
8
10
12
14
16
18
1/τφ (10^11/s)
T (K)
fit

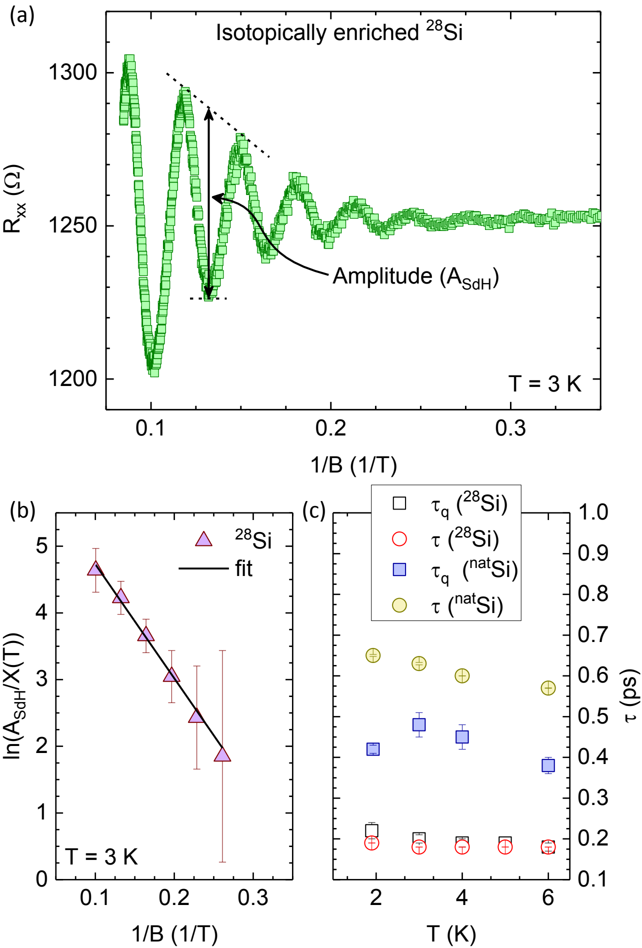

(a)
Isotopically enriched ^{28}Si
1300
1250
1200
R_{xx} (Ω)
Amplitude (A_{SdH})
T = 3 K
0.1
0.2
0.3
1/B (1/T)
(b)
^{28}Si
fit
T = 3 K
$\ln(A_{SdH}/X(T))$
1/B (1/T)
(c)
τ_q (^{28}Si)
τ (^{28}Si)
τ_q (^{nat}Si)
τ (^{nat}Si)
τ (ps)
T (K)